NUMERICAL ANALYSIS OF PRESSURIZED COLD BEND PIPES UNDER BENDING TO INVESTIGATE THE TRANSITION FROM COMPRESSION TO TENSION SIDE FAILURES

Celal Cakiroglu
Department of Civil and Environmental Engineering, University of Alberta
Edmonton, Alberta, Canada

Samer Adeeb
Department of Civil and Environmental Engineering, University of Alberta
Edmonton, Alberta, Canada

J. J. Roger Cheng
Department of Civil and Environmental Engineering, University of Alberta
Edmonton, Alberta, Canada

Millan Sen
Enbridge Pipelines Inc.
Edmonton, Alberta, Canada

ABSTRACT

The cold bended parts of pipelines are prone to geotechnical movements due to discontinuous permafrost, slope instabilities and seismic activities. Sen et al **[1]** carried out an extensive experimental study in 2006 in order to understand the buckling behaviour of cold bend pipes under applied curvature. In one of the experiments in this study, a high pressure X65 pipe specimen failed under applied curvature due to tension side fracture. This fracture was observed after the development of a wrinkle on the compression side. In this paper the behaviour of this cold bend pipe specimen under applied curvature and bending is investigated using finite element method to understand the conditions leading to pipe body tension side fracture in the post-buckling phase of a cold bend. The finite element analyses with and without internal pressure and the plastic strain and von Mises stress distributions showed that the tension side fracture occurs under equal amount of applied curvature only in the case of the pressurized pipes. These results were in accordance with the experimental results obtained by Sen et al **[1]** . The effect of internal pressure is analyzed further in order to determine a transition point of the mode of failure from compressive to tensile. A parametric study is conducted for a series of internal pressure values ranging from 20% Specified Minimum Yield Strength (SMYS) to 80% SMYS. A failure criterion based on the equivalent plastic strain reaching a critical value was used to assess the models behavior up to failure. It was observed that load cases having an internal pressure less than or equal to 60% SMYS exhibit higher equivalent plastic strains on the compression side throughout the simulations and up to failure. However, for internal pressure values higher than or equal to 67% SMYS the equivalent plastic strain on the tension side of the cold bend starts increasing dramatically at some point during the loading process exceeding the equivalent plastic strain values on the compression side up to failure.

1 INTRODUCTION

Excessive external loading in the form of tensile and bending forces can cause severe damages to pipelines. The main causes of these external loads are changes in the geotechnical conditions. Examples of such changes include differential settlement of the soil due to discontinuous permafrost, soil slope instabilities, soil swelling or soil liquefaction during an earthquake. Also temperature gradients between the operating temperature of the pipeline and the ambient temperature can cause damages to the pipe material.

In order to change the direction of a pipeline to conform to the terrain conditions, cold bending procedure is applied using a bending machine. The procedure causes significant changes in the material properties as well as the cross sectional geometry of the pipe. The distortion and ovalization in the cross sectional geometry of the pipe is proportional to the decrease in the radius of curvature. Another effect of cold bending on the pipe geometry is the increase in the pipe wall thickness at the intrados which is loaded in compression and the decrease of the pipe wall thickness at the extrados which is loaded in tension [2].

Besides the changes in the geometry of the pipe, cold bending procedure also causes residual stresses and material plastification by loading the intrados and the extrados beyond the yield stress in compression and tension respectively. As a result significant changes in the tensile properties of the pipe material are observed. Experimental studies carried out by Caminada et al [2] on cold bends with an R/OD ratio of 4.5 and grade T92 showed a 22% increase of the yield strength at the extrados and 18% decrease of the yield strength at the intrados [2].

Sen et al., [1] , [3] , [5] carried out eight full scale tests with cold bends of grades X60, X65 and X80 under in-plane bending and internal pressure. The general setup of these experiments is shown in Figure 1a. In this testing program the load /displacement responses of cold bend pipes with different configurations were analyzed. It was found that local buckling of cold bends takes place at lower strain values compared to straight pipes. The critical buckling strain for the cold bend pipes was on average 57% of the critical buckling strain for a straight pipe. This experimental study also

included tests with and without internal pressure which is another factor that influences the critical local buckling strain significantly. According to [3] the unpressurized specimens have critical strain values between 23% and 45% of that of a pressurized pipe. The failure modes in these full scale tests were, either failure due to fracture at the compression side of the wrinkles or buckling and a magnification of the imperfection patterns without fracture, except one NPS30 X65 specimen. This specimen suddenly fractured on the tension side of the wrinkle in the post-buckling phase under in-plane bending and an internal pressure corresponding to 80% SMYS hoop stress (Figure 1b).

Similar full scale tests were carried out by Miki et al [6] which applied opening mode and closing mode bending on cold bended pipes of grade X65. In these experiments which included pressurized and non-pressurized specimens, the ultimate strength of the cold bends were investigated based on the initiation of a crack on the pipe surface. It was found that the internal pressure significantly decreases the ultimate strength. In the closing mode bending case which is similar to Sen et al., [1] , [3] , [5] experimental configuration, it was observed that the pipe specimens did not crack even after reaching the maximum displacement capacity limit of the loading apparatus. The specimens only cracked during the unloading process. However, the applied internal pressure during Miki's experiment corresponded to a mere 40% SMYS hoop stress which is half the value that caused tensile fracture in Sen's experiments [1] .

The loading and pipe configurations leading to the tensile side fracture of Sen's experiment was further analyzed in a numerical study by Cakiroglu et al. [4]. In their study, four different levels of internal pressure corresponding to 70.6% SMYS, 73.8 % SMYS, 76.9% SMYS and 80% SMYS hoop stresses were applied. Similar load – displacement response was observed for these levels of internal pressure. Using the maximum equivalent plastic strain as a failure criterion, all the modeled levels of internal pressure caused tension side fracture albeit at different time instants during the loading process.

In this current work, the full scale experiment which was carried out by Sen [1] and resulted in the tension side fracture of a cold bend, is analyzed further using a numerical model similar to that employed by Cakiroglu et al. [4]. The main purpose of this current work is to investigate the level of internal pressure above which there is a risk of tensile fracture of cold bend pipes. For this purpose the cold bend configuration is numerically analyzed using finite element analysis under ten different levels of internal pressure in combination with applied displacement loading which increases the curvature of the cold bend. The analyzed internal pressure values correspond to a range of hoop stress values between 20% SMYS and 80% SMYS. The maximum equivalent plastic strain is chosen as a failure criterion to differentiate between tensile and compression side fractures. In addition, the variation of the plastic dissipated energy of the system is compared.

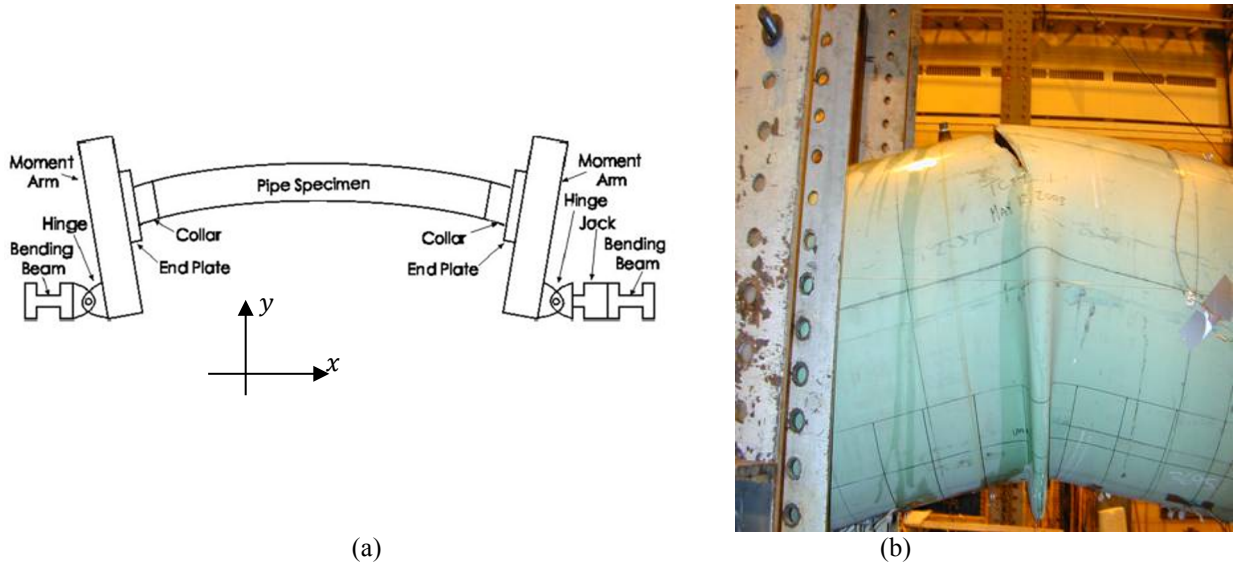

(a) (b)

Figure 1: (a) Schematic of the experimental setup by Sen et al. [3] , (b) Compression side wrinkle and tensile side fracture of a test specimen by Sen [1]

2 METHODS

The experimental setup (Figure 1a) of Sen [3] which resulted in a tension side fracture after the formation of wrinkles in the compression side of a cold bend by a combination of applied bending and internal pressure were simulated using the finite element analysis software ABAQUS. In the experimental setup, internal pressure was first introduced using water. After reaching the required level, a closing mode bending was applied on the cold bend using an I-section moment arm connected to a bending beam (which is referred to as the **loading pin**) located below the pipe axis (Figure 1a). The bending beam applied a horizontal displacement on the rigid moment arm, thus causing a closing bending loading on the specimen. A collar part was used near the end plates to prevent buckling at that location.

The geometric properties of the full scale specimen under consideration are listed in Table 1. In all simulations a 237 mm long section of the pipe next to the end plate is assigned a greater wall thickness (16 mm) than the rest of the model (8.2 mm). 4-node general purpose shell elements with reduced integration (S4R) were chosen to model the pipe geometry. The moment arm is modeled using rigid beam and multi point constraints. The nodes on the pipe edge are connected to the centroid of the cross section of the pipe edge using multi-point constraints. This node, in turn, was connected to another node 600 mm below this node with rigid beam constraints. The node which is located 600 mm below the pipe axis represents the loading pin.

In our models, for the sake of computational efficiency, the symmetry of the specimen around the $y-z$ and $x-y$ planes (Figure 1a) was used which enabled modeling only one quarter of the entire geometry. Symmetry boundary conditions were applied on the two symmetry planes. Loading was applied in two steps. In the first step, the required internal pressure was applied on the internal surface of the specimen. During this stage, the loading pin was fixed in place except for allowing it to rotate around the z axis. In the second step, the internal pressure was kept constant and a horizontal displacement was applied on the loading pin while allowing it to freely rotate around the z axis.

The simulated pipe specimen material was of grade X65 with SMYS of 448MPa and an ultimate strength of 531MPa. The material response after plastification was simulated using a metal plasticity model with isotropic hardening. The relationship between the equivalent stress and the equivalent plastic strain was assumed to be linear with the SMYS corresponding to zero equivalent plastic strain and the ultimate strength corresponding to 5% equivalent plastic strain. 10 different simulations were performed with internal pressure values ranging from 1.93 MPa (corresponding to 20% SMYS hoop stress) to 7.7 MPa (corresponding to 80% SMYS hoop stress) with equal steps. These simulations were also compared to a simulation without an internal pressure. The results for the equivalent stress (von Mises stress), equivalent plastic strain, the total plastic strain energy dissipated and the applied load on the loading pin were compared among the various models. A failure criterion of 40% equivalent plastic strain was utilized to indicate material failure.

Table 1: Geometric properties of the full scale specimen

Outer section diameter [mm]	762
Diameter to wall thickness ratio	93
Nominal wall thickness [mm]	8.2
Thickness of collar reinforced sections [mm]	16
Length of the collar reinforced sections [mm]	237
Total length [mm]	7454
Horizontal length [mm]	7400
Initial bend angle [degrees]	12
Initial radius of curvature [mm]	17796
Initial curvature [mm^{-1}]	5.62×10^{-5}

In the current work the curvature of the cold bend is calculated based on the assumption that as the displacement of the loading pin (u) is applied, the cold bend deforms into a circular arc with a radius of curvature (R). The nonlinear relationship between u and R is a function of the total length of the cold bend (L), the bend angle ($\theta = \frac{L}{2R}$) and the initial horizontal length of the cold bend (H_0) as follows:

$$2 \cdot R \cdot \sin\left(\frac{L}{2R}\right) = H_0 - u$$

As the curvature of the cold bend ($\kappa = \frac{1}{R}$) is a better measure for the cold bend deformation, for each applied u, the corresponding R was obtained by numerically solving the above equation. For the derivation of the expression for κ the reader is referred to [7]. The numerical algorithm makes use of the fact that the initial radius of curvature R_0 is known

and that increasing u decreases R (Figure 2). Using the curvature allows the generalization of the results to different pipe configurations having the same curvature. The obtained relationship between the applied displacement u and the curvature of the pipe κ is illustrated in Figure 3. In the rest of this paper, for each displacement of the loading pin the corresponding curvature value is used as a measure of deformation since the applied displacement value is dependent on a specific pipe configuration but the usage of the curvature value generalizes the obtained results.

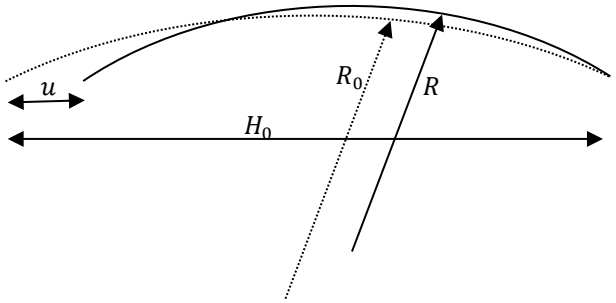

Figure 2: The original (undeformed) cold bend with an initial radius of curvature $\boldsymbol{R_0}$ (dotted lines) versus the deformed cold bend after applying a horizontal displacement $\boldsymbol{u}$ and the new radius of curvature $\boldsymbol{R}$.

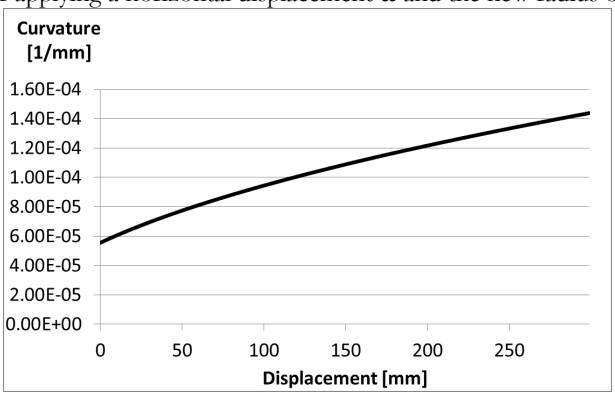

Figure 3: The relationship between the curvature $\boldsymbol{\kappa}$ and the applied displacement $\boldsymbol{u}$

3 RESULTS

3.1 Unpressurized case:

For the non-pressurized load case the pipe deformed with a diamond shaped wrinkle at the compression side of the cold bend in the post-buckling phase. The distribution of the equivalent plastic strain and the von Mises stress at the end of applying 300mm displacement is shown in Figure 4. The maximum von Mises stress and equivalent plastic strain values occur at the intrados of the wrinkle location. It can be observed in Figure 4b that the ultimate stress of the pipe base metal is reached at the compression side of the wrinkle location. The load/curvature plot in Figure 5 shows that the highest loading pin reaction force of 1.14×10^{6} N is reached at a relatively early stage of the simulation for a curvature value of 6.21×10^{-5} 1/mm. This peak reaction force is followed by a decrease in the load carrying capacity and stiffness which is accompanied by formation and magnification of a diamond shaped wrinkle on the compression side.

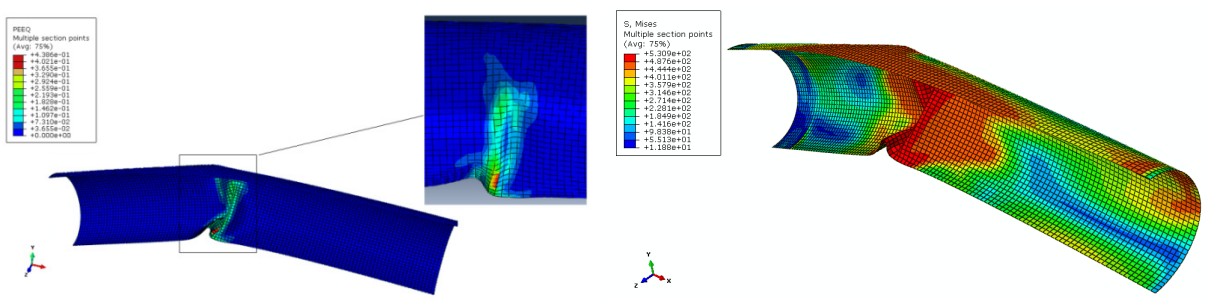

(a) (b)

Figure 4: (a) Equivalent plastic strain distribution and (b) von Mises Stress under bending load without internal pressure

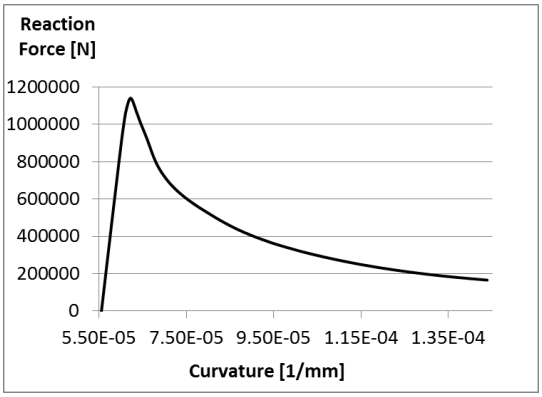

Figure 5: Load - displacement response under bending load without internal pressure

3.2 Pressurized cases:

For the internal pressure corresponding to 80% SMYS hoop stress, the models show a material failure at the tension side after the formation of a compression side wrinkle. Figure 6 shows the distributions of the equivalent plastic strain and the von Mises stress for this load case after applying a 299mm horizontal displacement. This corresponds to a curvature of the pipe axis of value 1.44×10^{-4} 1/mm.

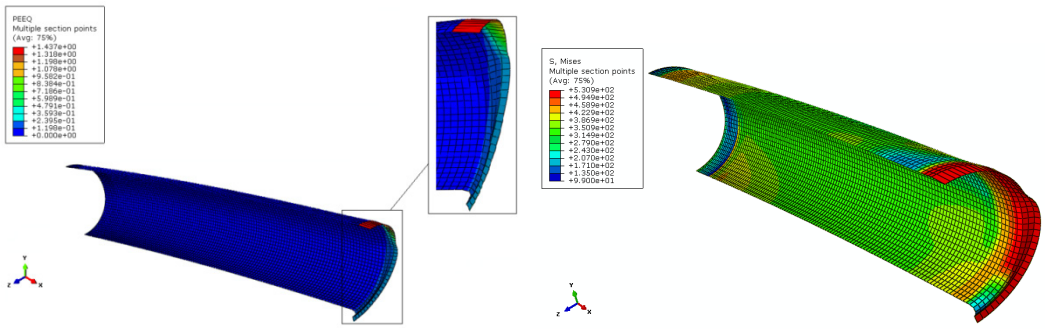

(a) (b)

Figure 6: (a) Equivalent plastic strain distribution and (b) von Mises Stress under bending load with internal pressure corresponding to 80% SMYS hoop stress

Figure 6 shows considerably high values for the equivalent plastic strain and the von Mises stress concentrated at the tension side of the wrinkle location for the load case with internal pressure corresponding to 80% SMYS hoop stress. At the tension side, the element shapes are highly distorted which is an indication of tensile strain values beyond what the material can withstand.

The data representing the load-displacement response for each load case is shown in Figure 7. It was observed that there is a decrease in the peak reaction force at the loading pin as the internal pressure increases from 20% SMYS to 67% SMYS (Figure 7). In this range of internal pressure (20% - 67%SMYS) there is a clear peak reaction force which indicates the transition into the post-buckling phase. Whereas for the internal pressure values above 67% SMYS there is no sharp transition to the post-buckling phase which can be a result of an increase of the post-buckling global stiffness of the structure due to the high internal pressure values. In Figure 7 the straight black line marks the peak reaction forces which are regarded as transition points into the post-buckling phase for each load case having an internal pressure value of up to 67% SMYS. From Figure 7, it can be clearly observed that as the internal pressure increases from 20% SMYS to 67% SMYS the peak reaction force linearly and continuously decreases. In load cases having an internal pressure greater than 67% SMYS, the reaction forces continuously increase until failure without any indication of unstable behaviour or negative slopes in the force- displacement curves.

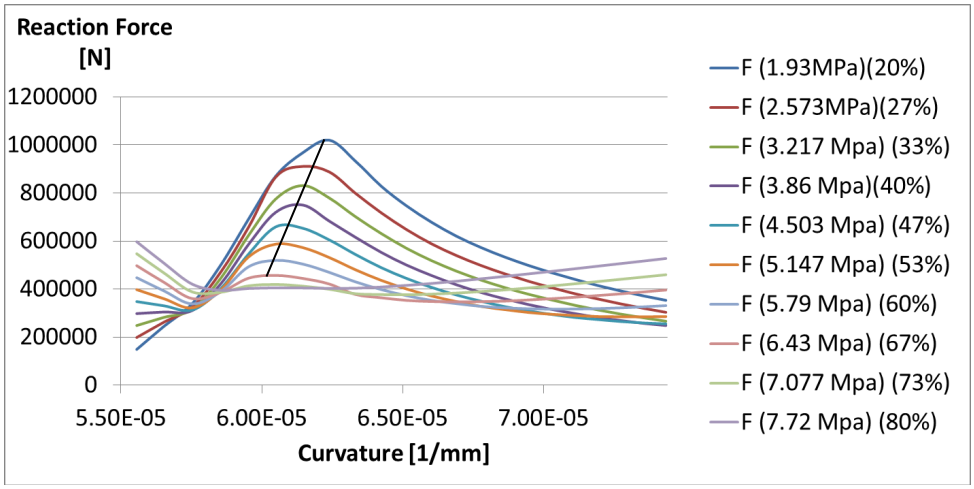

Figure 7: Variation of the reaction force at the loading pin with respect to displacement for each internal pressure

In order to understand the relationship between the development of the equivalent plastic strain and the internal pressure, the development of the equivalent plastic strain value is visualized for the selected values of the internal pressure. The development of the equivalent plastic strain on both the tension and compression sides and the plastic dissipation energy with respect to increasing the curvature is illustrated for the cases with internal pressure corresponding to 20%, 60%, 67% and 80%SMYS hoop stress (Figure 9). For the 20% case (Figure 9a), the equivalent plastic strain on the compression side increases during the early stages of the analysis. On the other hand, the equivalent plastic strain on the tension side develops at a later stage in the analysis and increases at a much slower rate. When the compression side equivalent plastic strain reaches 40% (the designated failure criterion), the value of the equivalent plastic strain on the tension side is around one eighths of that value (4.82%). The same behavior is observed for the 60% case (Figure 9b), however, the equivalent plastic strain on the tension side is higher (29.5%).

Figure 9c,d show that for 67% SMYS and 80% SMYS internal pressure values the behavior of the pipe is similar to the cases with lower internal pressure up to a curvature of around 9.5×10^{-5} 1/mm. Beyond this curvature, the rate of increase of the equivalent plastic strain on the compression side decreases and the value of the equivalent plastic strain never reaches the 40% failure criterion. On the other hand, the equivalent plastic strain on the tension side increases with a much faster rate overpassing the equivalent plastic strain on the compression side and reaching the 40% designated failure criterion. The point at which both the tension and compression side equivalent plastic strains are equal occurs at the curvature values of 12.9×10^{-5} 1/mm and 11.4×10^{-5} 1/mm for the 67% and 80% cases respectively.

By picking the intermediate curvature value of 9.5×10^{-5} 1/mm, the equivalent plastic strain is 33.5% on the compression side and 3.54% on the tension side for the 20% case. For the same value of curvature in the load case of 60% SMYS internal pressure the equivalent plastic strain is 30.5% on the compression side and 4.8% on the tension side. This indicates that as the internal pressure increases from 20% SMYS to 60% SMYS, for the same curvature, the maximum equivalent plastic strain value decreases at the compression side and increases at the tension side. Similarly, for the internal pressure of 67% SMYS the equivalent plastic strain on the compression side is 29.8% and the equivalent plastic strain on the tension side is 5.8%. For the case of 80% SMYS internal pressure the equivalent plastic strain on the compression side decreases to 28.6% and the equivalent plastic strain on the tension side increases to 6.8%. The

accumulated equivalent plastic strain on the compression and tension sides at the fixed curvature of 9.5×10^{-5} 1/mm is visualized in Figure 12.

Figure 8 shows the curvature of the cold bend when 40 % equivalent plastic strain failure criterion is reached whether it is on the tension or compression sides. For the load cases of 67% to 80% SMYS (zone 2) the equivalent plastic strain reaches the 40% value on the tension side. However, for these load cases, the equivalent plastic strain value on the compression side approaches 40% asymptotically as the curvature increases. On the other hand, for the load cases of 20% to 67%, the equivalent plastic strain reaches 40% on the compression side but not on the tension side. These results indicate that an increase of the internal pressure upto and beyond the 67% SMYS is coupled with an earlier onset of failure on the tension side.

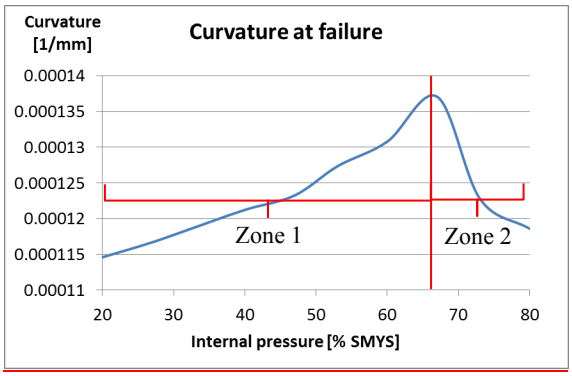

Figure 8: The relationship between the applied curvature in [1/mm] at failure (using the 40% equivalent plastic strain failure criterion) and the internal pressure.

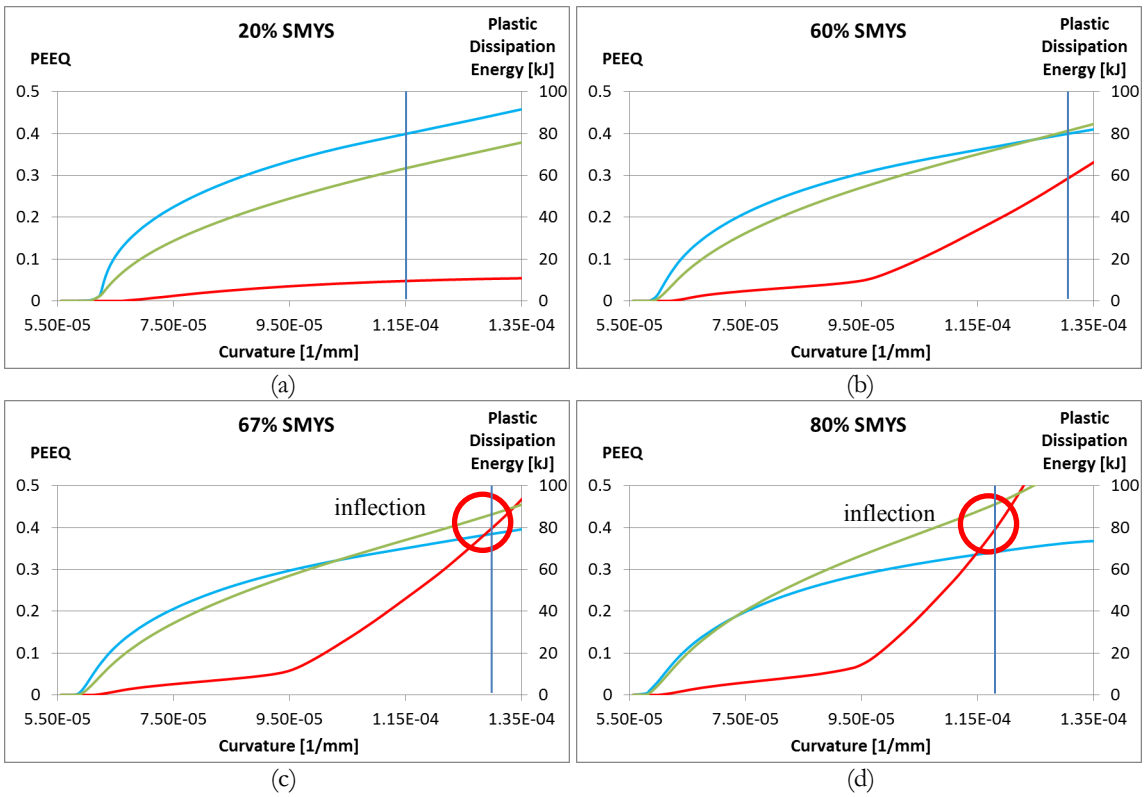

Figure 9: Development of the equivalent plastic strain at the compression side (blue), at the tension side (red) and the plastic dissipation energy (green) with respect to increasing curvature for the cases of internal pressure corresponding to (a) 20%, (b) 60%, (c) 67% and (d) 80%SMYS hoop stress

The amount of plastic energy dissipated throughout the simulations for the 20%, 60%, 67% and 80% SMYS load cases as a function of the applied curvature is shown in Figure 9. For 20% SMYS and 60% SMYS internal pressure cases the plastic dissipation energy curves follow a very similar course as the equivalent plastic strain curves of the compression side whereby the rate of change (slope) of the dissipated plastic energy is decreasing. However, for the 67% and 80%, the curves of the plastic energy are characterized by an inflection point beyond which the slope starts increasing. In Figure 9 c,d the red circles show the inflection points of the green curves. The location of these inflection points is in accordance with the designated failure criterion of 40% equivalent plastic strain. In Figure 9 c,d the inflection of the green curves occur when the applied curvature is between $1.15 \cdot 10^{-4}$ 1/mm and $1.35 \cdot 10^{-4}$ 1/mm. This is the range of curvature where the equivalent plastic strain reaches the level of 40% on the tension side for the load cases between 67% SMYS and 80% SMYS internal pressure. This observation shows that the plastic dissipation energy curve could be used to make inferences about a possible tension side failure.

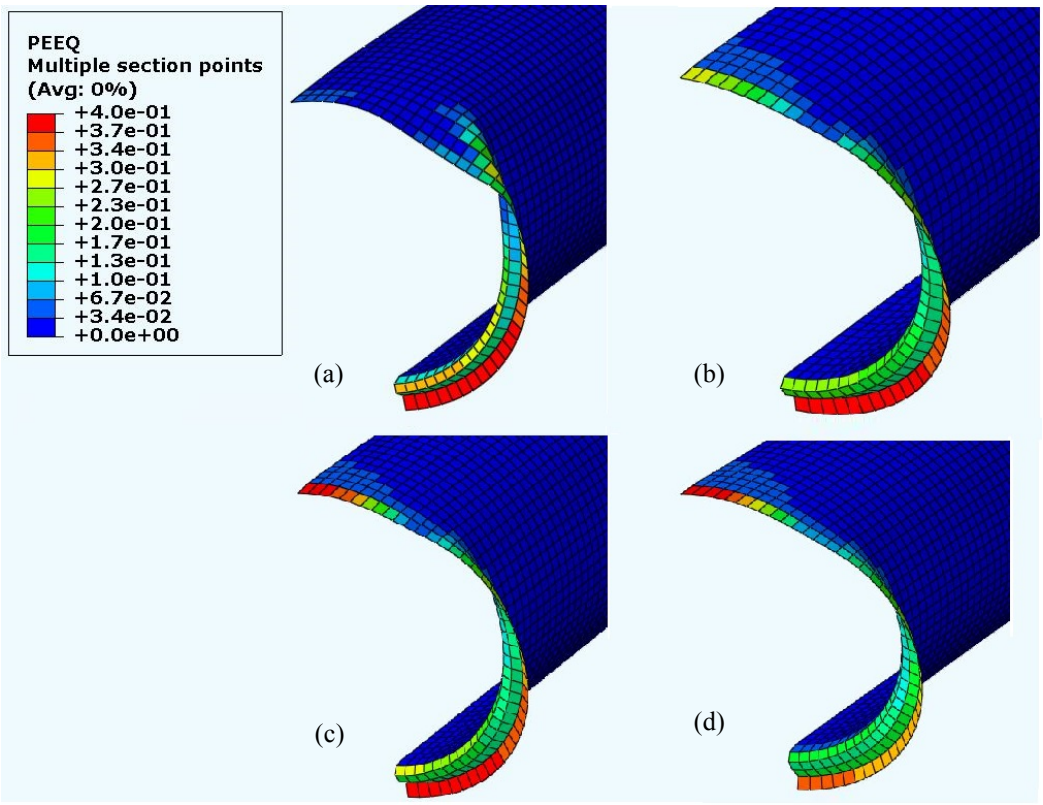

Figure 10: Distribution of the equivalent plastic strain at the wrinkle location at failure for the load cases of internal pressure corresponding to (a) 20%, (b) 60%, (c) 67% and (d) 80% SMYS hoop stress

Figure 10 shows the equivalent plastic strain distributions at the wrinkle location for 20% SMYS, 60% SMYS, 67% SMYS and 80% SMYS internal pressure when the maximum equivalent plastic strain reaches 40%. As shown in the figure, there is a clear difference between the equivalent plastic strain at the tension (top) side and that at the compression (bottom) side. For the cases of 20% and 60%, the equivalent plastic strain in the tension side is well below the 40% failure criterion, while that at the compression side is close to the 40% equivalent plastic strain failure criterion. When the internal pressure is increased to 67% and 80% SMYS hoop stress, the situation is reversed. The equivalent plastic strain on the tension side exceed the 40% while that on the compression side is below that level in the 67% case and is even much lower in the 80% case.

Figure 11a shows the development of the equivalent plastic strain on the tension side of the wrinkle location for a variation of the internal pressures between 20% and 80% SMYS hoop stress. As shown in the figure, the internal pressure cases 67% SMYS through 80% SMSYS have dramatically increasing equivalent plastic strain values at curvatures greater than 9.4×10^{-5} 1/mm. On the other hand Figure 11b shows the development of the equivalent plastic strain on the compression side of the wrinkle location for the same range of internal pressure values. As shown in the figure, the development of the plastic strain on the compression side is similar for all internal pressure levels albeit with a slight decrease in the values with the increase in the internal pressure levels. In particular, for the 67% through 80% load cases, the values do not reach the 40% equivalent plastic strain failure criterion.

As shown in Figure 11, the equivalent plastic strain on the tension side and the compression side at the initial stages of loading is similar for all the internal pressure levels. This is illustrated by plotting the maximum equivalent plastic strain on the tension and compression side as a function of the internal pressure level at the specific curvature value of 9.5×10^{-5} 1/mm (Figure 12a). At this curvature level, the equivalent plastic strain at the compression side drops slightly from 34% to 29% as the internal pressure level increases from 20% to 80%. Similarly, at the curvature level of 1.25×10^{-4} 1/mm the equivalent plastic strain at the compression side drops from 40% to 35% (Figure 12b). At the same time, the equivalent plastic strain at the tension side at the lower curvature value (Figure 12a) increases slightly from 4% to 6.5% as the internal pressure level increases from 20% to 80%. However, at the higher curvature of 1.25×10^{-4} 1/mm, the internal pressure level causes a drastic increase in the equivalent plastic strain in the tension side (Figure 12b) from 5% at the 20% internal pressure level to an equivalent plastic strain of 55% (well above the 40% failure criterion) at the 80% internal pressure level.

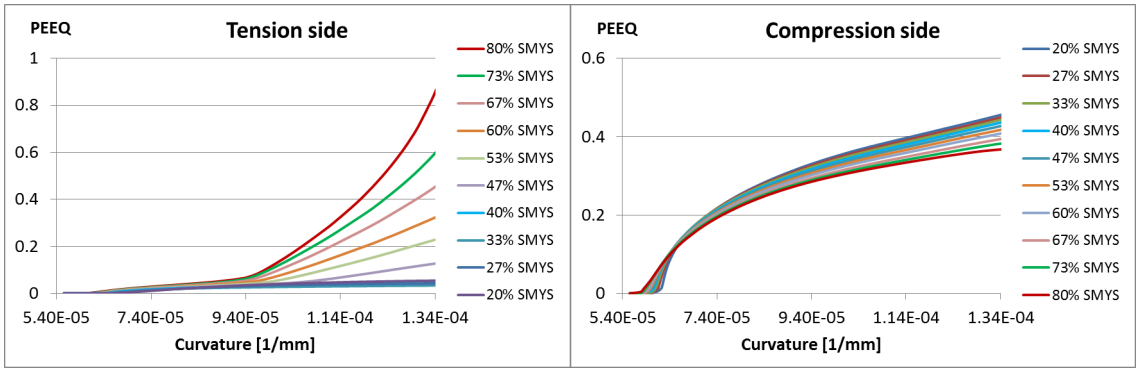

(a) (b)

Figure 11: Development of the equivalent plastic strain on the (a) tension side and (b) compression side of the wrinkle location at different values of the internal pressure

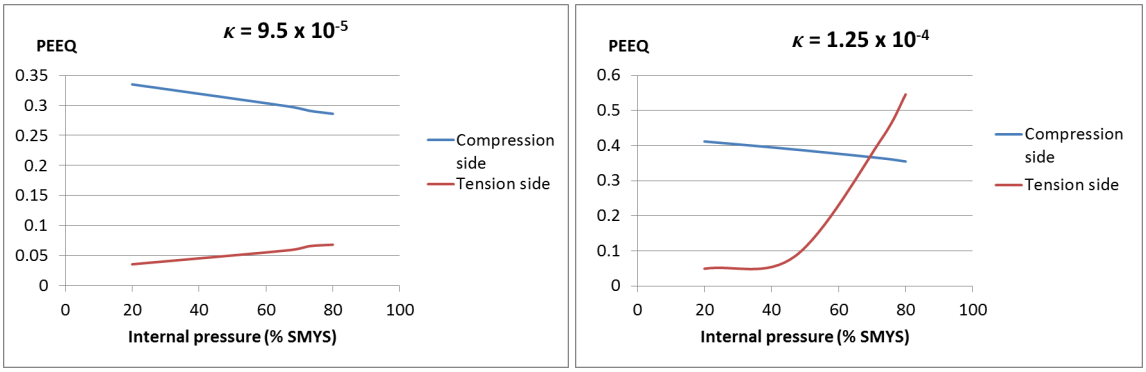

(a) (b)

Figure 12: Variation of the equivalent plastic strain with respect to internal pressure at the compression and tension sides for curvatures of (a) 9.5×10^{-5} and (b) 1.25×10^{-4} 1/mm.

4 DISCUSSION AND SUMMARY

In the process of transporting oil and gas from the source to the location of consumption, pipelines have proven to be the most efficient method of transportation. In this process pipe direction is necessarily changed in a horizontal or vertical plane according to the changes in the terrain conditions. Changes in the pipe direction are achieved often by applying a cold bending process which causes an accumulation of residual stresses at the cold bend locations. These residual stresses make the cold bend locations of a pipeline prone to structural failure in the form of fracture or buckling. Substantial external forces are applied on the cold bends in case of unstable ground movements like slope instability or differential settlement due to discontinuous permafrost. Displacements caused by these ground movements lead to an accumulation of strains in the cold bend locations which can eventually lead to the formation of wrinkles. Because of this combination of residual stresses due to the cold bending process and the accumulation of strains due to the external forces, it is crucial to investigate the structural response of cold bends under external loading. In the scope of this work the structural response of a cold bend configuration is investigated in case of changing the curvature of the cold bend. The structural response is investigated for different values of internal pressure using a parametric study.

In the current work, the full scale test configuration of a cold bend which resulted in the loss of containment capability due to tension side fracture is investigated numerically. Particularly, the effect of increasing the internal pressure is analyzed. In all simulations a combination of internal pressure and displacement which increases the curvature of the cold bend is applied. In order to analyze the effect of internal pressure, a parametric study is carried out which encompasses internal pressure values causing a range of hoop stresses between 20% SMYS and 80% SMYS. The visualization of the results showed that two different types of structural response are occurring as the internal pressure of the cold bend increases. The first type of structural response is observed for internal pressure values between 20% SMYS and 67% SMYS. This type of response is characterized by a relatively sharp transition to the post-buckling phase with a peak reaction force at the loading pin. The peak reaction force in this case is inversely proportional to the internal pressure. The second type of structural response is observed for internal pressure values corresponding to 67% SMYS and 80% SMYS. In these load cases the reaction forces increase continuously throughout the simulations and no peak reaction forces can be observed. It is concluded that the increase in the internal pressure leads to an increase in the global stiffness of the structure which prevents clearly recognizable global buckling.

In the next step of the analysis the variation of the equivalent plastic strain with respect to increasing curvature is compared for the various internal pressure levels. It is observed that as the internal pressure increases, the maximum equivalent plastic strain decreases on the compression side and increases on the tension side for any value of applied curvature. At lower applied curvature levels, these changes in the equivalent plastic strain are relatively small. However, at higher curvatures, there is a dramatic increase in the equivalent plastic strain on the tension side associated with the increase in the internal pressure level.

In addition to the variation of the equivalent plastic strain, also the change in the plastic dissipated energy is compared for the various internal pressure levels. Two different types of variation could be observed for the plastic dissipated energy. The first type of variation is observed for internal pressure values less than 67% SMYS. In this first variation, the plastic dissipation energy asymptotically increases throughout the simulation (Figure 9). In the second type of variation there is an inflection point in the curve showing the variation of the plastic dissipation energy as a function of applied curvature (Figure 9). In the second type of variation the inflection of the plastic dissipation energy curve occurs in the vicinity of the point where the equivalent plastic strain value at the tension side exceeds that at the compression side. At these inflection points the rate of change of the slope of the plastic dissipated energy curve changes from negative to positive. This behaviour is an indicator of an overall "yielding" of the pipe structure in which a slight change in the applied load is associated with a large amount of plastic energy dissipated in the structure. These two different types of variation occur in the same range of internal pressure values as the two different types of variation of the reaction force. Since starting from these inflection points higher strain values are observed at the tension side it can be concluded that for internal pressure values of 67% SMYS or higher the material failure in form of fracture is expected at the extrados of the cold bend.

One of the limitations of our study is the assumption of a perfectly circular cold bend axis in the calculation of the curvature. This assumption is valid at the initial stage of the analysis until the formation of a wrinkle at which point, it is perhaps better to use a different deformation measure. Another limitation in this study is related to the chosen failure criterion for the cold bend steel. We have chosen the failure criterion to be when the maximum equivalent plastic strain reaches 40%. In general, this reported value was reached in a single element in the discretized geometry. According to this criterion the pipe material failure is assumed to have occurred if at least one element has reached this strain level. This approach inevitably defines the failure of the pipe dependent on a particular geometric discretization. A more general approach could be to define the failure criterion based on the average equivalent plastic strain value in a predefined geometric domain.

Another limitation is that the development of the equivalent plastic strain with respect to increasing internal pressure is studied for a fixed geometric and material configuration. The transition of the failure mode from compression side to tension side could occur at different levels of internal pressure for different pipe configurations.

REFERENCES

[1] Sen M. (2006); "Behaviour of Cold Bend Pipes Under Combined Loads" Ph.D. dissertation, University of Alberta, 2006

[2] Caminada S, Cumino G, Cipolla L, Di Gianfrancesco, A (2009). "Cold bending of advanced ferritic steels: ASTM grades T23, T91, T92". International Journal of Pressure Vessels and Piping 86 (2009) 853–861

[3] Sen M., Cheng, J.J.R. , Zhou, J. (2011). " Behaviour of Cold Bend Pipes under Bending Loads" DOI: 10.1061/(ASCE)ST.1943-541X.0000219. 2011 American Society of Civil Engineers

[4] Cakiroglu C, Komeili A, Adeeb S, Cheng JJR, Sen M (2012). "Numerical Analysis of High Pressure Cold Bend Pipe to Investigate the Behaviour of Tension Side Fracture", IPC2012-90381

[5] Sen M, Cheng JJR, Murray DW (2004). "Full-Scale Tests of Cold Bend Pipes" Proceedings of IPC2004, International Pipeline Conference, IPC2004 – 743

[6] Miki C, Kobayashi T, Oguchi N, Uchida T, Suganuma A, Katoh A. (2000). "Deformation and fracture properties of steel pipe bend with internal pressure subjected to in-plane bending ". Proceedings of the 12th World Conference on Earthquake Engineering.

[7] Pressley A (2010). "Elementary Differential Geometry". ISBN: 978-1-84882-891-9